Multifunctional, Polymorphic, Ionic Fullerene Supramolecular Materials: Self-Assembly and Thermotropic Properties

ARTICLE *in* LANGMUIR · JUNE 2011

Impact Factor: 4.46 · DOI: 10.1021/la2015176 · Source: PubMed

6 AUTHORS, INCLUDING:

Hongguang Li
Chinese Academy of Sciences
44 PUBLICATIONS **523** CITATIONS
SEE PROFILE

Martin J Hollamby
Keele University
30 PUBLICATIONS **685** CITATIONS
SEE PROFILE

Shiki Yagai
Chiba University
108 PUBLICATIONS **2,908** CITATIONS
SEE PROFILE

Helmuth Moehwald
Max Planck Institute of Colloids and Interfaces
1,002 PUBLICATIONS **38,571** CITATIONS
SEE PROFILE

Langmuir

ARTICLE

pubs.acs.org/Langmuir

Multifunctional, Polymorphic, Ionic Fullerene Supramolecular Materials: Self-Assembly and Thermotropic Properties

Hongguang Li,[†] Martin J. Hollamby,[‡] Tomohiro Seki,[§] Shiki Yagai,[§] Helmuth Möhwald,[†] and Takashi Nakanishi*[,†,‡]

[†]Max Planck Institute of Colloids and Interfaces, 14424 Potsdam, Germany

[‡]National Institute for Materials Science (NIMS), 1-2-1 Sengen, Tsukuba 305-0047, Japan

[§]Chiba University, 1-33 Yayoi-cho, Inageku, Chiba 263-8522, Japan

Supporting Information

ABSTRACT: An *N*-methylfulleropyrrolidine (**2**) bearing three eicosyloxy chains on the laterally substituted phenyl group can be further functionalized to give the ionic fullerene derivative, i.e., *N*,*N*-dimethylfulleropyrrolidinium iodide (**1**). The spectroscopic, electrochemical, self-assembly, and liquid crystalline properties of **1** have been investigated and compared to its neutral precursor **2**. Changes in electronic structure upon ionization are observed in the UV spectra. Additionally, a positive potential shift of electrochemical reductions for **1** compared to those of **2** is noted in both homogeneous solution and film state. Driven by the $\pi-\pi$, van der Waals, and electrostatic interactions, the ionic compound **1** is able to form a variety of functional and polymorphic self-assembled structures both from solution and on substrates, including hierarchically organized flakelike microparticles with high water repellency, doughnut-shaped objects with rough surfaces, and long one-dimensional C_{60} nanowires (>1 μm). The thermotropic behavior of **1** has also been investigated, and a smectic liquid crystalline phase was observed at elevated temperatures. Further investigations of the thermotropic behavior of **1** revealed that a deionization back-reaction from **1** to the neutral precursor **2** gradually occurred. The mechanism of this deionization reaction is presented and discussed. These investigations provide insight into the effects of added ionicity to alkylated fullerene derivatives, in particular on their self-assembly features and functionality.

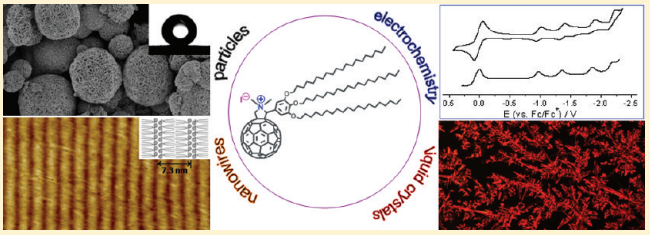

INTRODUCTION

Because of their combination of unique geometric and physicochemical properties, fullerenes (e.g., C_{60}) continue to be an exciting research topic in physics, chemistry, biology, and materials science.[1−5] As a good electron acceptor and an n-type semiconducting material, fullerene-based materials have great potential in optoelectronic applications. The construction of well-ordered self-organized structures where C_{60} moieties have long-range order is thought to be crucial to reach high carrier mobilities.[6,7] To obtain such ordered materials, the ability to fine-tune the interactions between neighboring C_{60} molecules is of critical importance. One solution to this problem could be the attachment of substituent groups by suitable synthetic procedures. For any potential applications to be realized, simple synthetic procedures with minimum steps and high yields are desirable.

Among various C_{60} derivatization routes, the Prato reaction,[8] which belongs to the [3 + 2] cycloaddition pattern, has been proved to be very powerful, with high yields of molecules with interesting properties such as high stability under electrochemical reductions.[9] A further advantage of the Prato route is that the neutral fulleropyrrolidines can be ionized by a simple quaternization reaction, which introduces a positive charge onto the nitrogen atom of the pyrrolidine ring. This significantly enhances the water solubility of the resulting ionic C_{60} derivatives (fulleropyrrolidinium), rendering them suitable for biological tests both *in vitro* and *in vivo*.[10,11] Because of the zwitterion formation between the C_{60} moiety and the pyrrolidine ring,[12] fulleropyrrodiniums are more photostable than their neutral precursors and their ability to accept electrons from donor molecules is greater. The layer-by-layer technique can also be used on fulleropyrrolidiniums, in combination with negatively charged polyelectrolytes, to form functional films.[13,14] Consequently, fulleropyrrolidinium compounds are considered to be potentially useful substances for optoelectronic applications.

Recently, the syntheses of a variety of alkylated *N*-methylfulleropyrrolidines via merely two synthetic steps (including the Prato reaction) have been reported alongside further studies of their materials and supramolecular chemistries.[15−21] The aliphatic chains are grafted onto the pyrrolidine ring via a lateral phenyl group. Although both C_{60} and aliphatic chain units are considered to be hydrophobic, their polarities are different and they are mutually immiscible.[16] This allows these molecules

Received: April 24, 2011
Revised: May 10, 2011
Published: May 20, 2011

Scheme 1. Synthesis of Alkylated *N,N*-Dimethylfulleropyrrolidinium Iodide (1) from Its Neutral Precursor, Alkylated *N*-Methylfulleropyrrolidine (2)

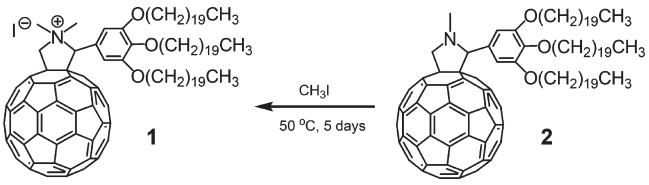

("hydrophobic amphiphiles") to exhibit versatile self-organized architectures with supramolecular polymorphism when processed using different combinations of organic solvents.[17] Within these structures, the immiscible units segregate, typically into lamellar phases, with an alternate arrangement of C_{60} and aliphatic chains.[18,19] A good example of the establishment of long-range ordering was observed on a graphite surface, where self-organized C_{60}-nanowires were formed due to a balance of interactions between the surface and between individual molecules.[20] By altering the aliphatic chain group, some alkylated *N*-methylfulleropyrrolidines have been found that act as thermotropic liquid crystals possessing a high C_{60} content (up to 50%) with relatively high carrier mobility.[20] These molecules, alongside various other alkylated C_{60} derivatives[22−27] for which the focus is typically the generation of soft fullerene-containing materials such as organogels,[25] liquid crystals,[26] and OFET components,[27] are therefore naturally of current interest for a wide range of organic electronic applications.

Here, by combining the two previously described approaches, an ionic moiety is introduced onto the alkylated *N*-methylfulleropyrrolidines to form corresponding alkylated *N,N*-dimethylfulleropyrrolidiniums. This induces an electrostatic interaction to the assemblies, in addition to the van der Waals forces present and the $\pi-\pi$ interaction between neighboring C_{60} molecules. Ionic supramolecular systems possessing π-conjugated moieties are known as one of the new generations of organic functional materials[28−30] and have found use as electrochromic liquid crystals,[31] actuators,[32] anion-responsive gels,[33] and metal nanostructured templates.[34] Here, we focus on the self-assembly and thermotropic properties of the new alkylated *N,N*-dimethylfulleropyrrolidinium compounds. Typically **1**, bearing three eicosyloxy chains on the phenyl substituent and with an iodine anion as counterion, was synthesized as a model molecule (Scheme 1). To better highlight the specific contribution of the ionic moiety, comparisons with the neutral precursor, **2**, are presented and discussed throughout the work. In doing so, we present a new category of supramolecular fullerene materials, which form multifunctional polymorphic materials based on the self-assembly of ionic alkylated fullerenes.

EXPERIMENTAL SECTION

Materials. 1-Bromoeicosane (98%), 3,4,5-trihydroxybenzaldehyde (98%), C_{60} (99.5%), sarcosine (>99%), and K_2CO_3 (>99%) were purchased from Sigma-Aldrich and used as received. KI (99%) and methyl iodide (99%, stabilized with copper or silver) were purchased from Alfa Aesar and used without further purification. The synthesis and characterization of alkylated *N*-methylfulleropyrrolidine **2** was carried out following reported procedures[20] with a better yield up to 47.5% based on the conversion of C_{60} (previous yield in ref 19 is 35.2%).

Synthesis of 1. To a 100 mL round-bottom flask containing 50 g of methyl iodide (CH_3I), 100 mg (0.057 mmol) of **2** was added. The reaction was continuously stirred at 50 °C for 5 days. The reaction mixture was cooled to room temperature, and the excess CH_3I was removed under reduced pressure. The crude product was then purified by silica gel column chromatography (eluent: 10% MeOH in CH_2Cl_2) to remove unreacted **2**. The final product **1** was obtained as a yellow-brown solid (70 mg, yield: 70%). ^{1}H NMR (400 MHz, 10% CD_3OD in $CDCl_3$): δ 7.23−7.02 (2H), 6.07 (1H, J = 12.8 Hz), 5.88 (1H, J = 12.8 Hz), 4.30−4.20 (3H), 4.18−3.92 (6H), 3.92−3.84 (3H), 1.90−1.60 (6H), 0.95−0.80 (9H). FT-IR (KBr, cm^{-1}): 2921, 2851, 1586, 1507, 1465, 1333, 1247, 1116. MALDI-TOF-MS: calculated: 1758.5; found: 1758.3.

Instruments and Methods. NMR spectra were recorded on a Bruker DMX400. MALDI-TOF-MS spectra were recorded on a Shimadzu Axima Confidence. The matrix used is 2-(4-hydroxyphenylazo)-benzoic acid. UV−vis spectra were measured on a Varian Cary50 Conc spectrophotometer. Scanning electron microscope (SEM) images were recorded using a Philips XL30 electron microscope at an accelerating voltage of 3 kV. Before measurements the samples were sputtered with Au in a JFC-1300 JEOL automatic sputter coater equipped with a MTM-20 thickness controller. Atomic force microscope (AFM) investigations were carried out with a Nanoscope IIIa (Veeco) in tapping mode. Si cantilevers (length 122 μm and width 25 μm) with spring constants between 25 and 42 N m^{-1} were used. X-ray diffraction (XRD) patterns were measured using a Rigaku RINT Ultima III X-ray diffractometer with monochromatic Cu Kα radiation (λ = 0.154 nm). Small-angle X-ray scattering (SAXS) measurement was carried out on a self-built setup (rotating anode Fr 591, Osmic mirror, MARCCD detector) with Cu Kα radiation . The sample-to-detector distance was 25 cm, giving a measurable Q-range of approximately 1.0−6.2 nm^{-1} After 4 nm^{-1} no scattering was detected above the background, so the displayed data range was cropped to allow better visualization of the peaks. FT-IR spectra were recorded on a Bruker EQUINOX 55/S spectrophotometer using a KBr pellet. Differential scanning calorimetry (DSC) and thermogravimetric analysis (TGA) measurements were carried out using a DSC 204 (Netzsch) under nitrogen with a scanning speed of 10 °C/min. Contact angle measurements were implemented with a contact angle measuring system G10 (Krüss, Germany) at ambient temperature. Electrochemical experiments were conducted using a classic three-electrode system with a Gamry Reference 600 potentiostat/galvanostat/ZRA Instrument. A glassy carbon electrode was used as working electrode and a Pt ring was used as auxiliary electrode. For measurements in film state conducted at 70 °C, Ag/AgCl (saturated KCl) was used as the reference electrode. For measurements in CH_2Cl_2 solution conducted at room temperature, a Pt plate was used as the quasi-reference electrode and the ferrocene/ferrocenium (Fc/Fc^+) redox couple was used as internal reference for the potential calibration.

RESULTS AND DISCUSSION

Synthesis. 3,4,5-Tri(eicosyloxy)phenyl-*N,N*-dimethylfulleropyrrolidinium iodide (**1**) was synthesized by quaternization of a corresponding neutral molecule, its *N*-methylfulleropyrrolidine (**2**). Because of the reduced reactivity of the pyrrolidine nitrogen atom due to the nearby bulky C_{60} unit,[35,36] the reaction was carried out above room temperature (50 °C) with CH_3I acting as both reactant and solvent. Reactions carried out in a CH_3I/$CHCl_3$ mixed solvent and/or at room temperature gave low yields. After reaction for 5 days, a new spot appeared in the thin-layer chromatography analysis (TLC, eluent: 10% MeOH in CH_2Cl_2) with a lower R_f value than **2**. This was identified to be **1** by ^{1}H NMR and MALDI-TOF-MS analyses. While other fulleropyrrolidinium compounds with different functional groups

dx.doi.org/10.1021/la2015176 |*Langmuir* 2011, 27, 7493–7501

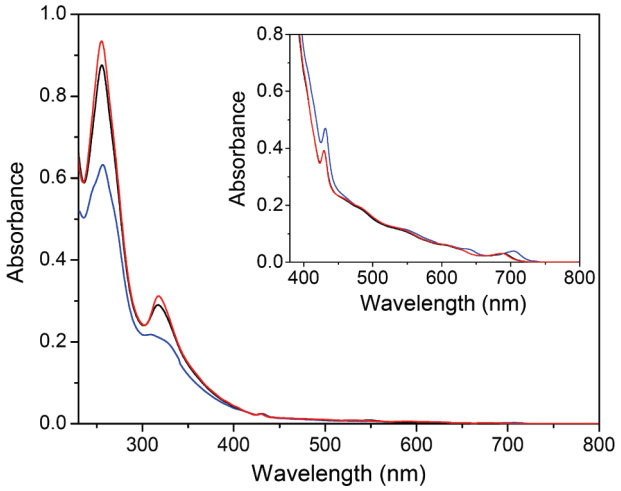

Figure 1. UV−vis absorption spectra of 5 μM **1** in CH_2Cl_2 (black) and a MeOH/CH_2Cl_2 mixed solvent with a MeOH volume content of 10% (red). The spectra of 5 μM **2** in CH_2Cl_2 (blue) is given for comparison. Insets are the spectra recorded using a concentration of 100 μM to highlight the absorptions in visible region.

have been reported in the past two decades,[10−14] they were all either water-soluble or had limited solubility in any common solvents. This made it difficult to purify them by column chromatography. Instead, washing with water is usually used to isolate these compounds which can result in loss of compound and in inadequate purity. Conversely, **1** is probably the first example of a fulleropyrrolidinium compound that can be isolated by simple, conventional silica column chromatography. This allowed a highly pure fulleropyrrolidinium salt **1** to be attained and also enabled monitoring for any possible changes (e.g., aging effects) during our experiments.

As can be expected, converting **2** to **1** induced an increase in hydrophilicity. Solubility tests revealed that **1** does not dissolve significantly in highly polar solvents like MeOH and water but (similarly to **2**) retains good solubility in a variety of organic solvents, including aromatic and relatively nonpolar solvents. This can be ascribed to the presence of the C_{60} and bulky lateral alkyl chain groups, which are both hydrophobic. Specifically, **1** can be readily solubilized in CH_2Cl_2, $CHCl_3$, THF, and toluene as well as mixtures of the above with alcohol. This significantly facilitates the solution characterization and also enables us to fabricate various multifunctional architectures via solution processes.

Spectroscopic Properties. UV−vis absorption spectra of **1** in CH_2Cl_2 (Figure 1, black curve) as well as in a MeOH/CH_2Cl_2 mixed solvent with a MeOH volume content of 10% (Figure 1, red curve) were carried out in comparison to its neutral precursor **2** (Figure 1, blue curve). Both **1** and **2** exhibit a variety of absorption peaks ranging from ultraviolet to visible region that are characteristic of C_{60} monoadducts.[37] Upon ionization from **2** to **1**, clear spectroscopic changes can be observed. These include (i) an increase of molar absorption coefficient in the UV region, (ii) a slight decrease of molar absorption coefficient in the visible region, (iii) a change in the broad absorption band around 317 nm to a sharp peak, and (iv) a blue shift of the peaks especially at longer wavelengths. These changes indicate that the ionization perturbs the electronic structures of the C_{60} moiety.[38] The spectra of **1** in MeOH/CH_2Cl_2 mixed solvent shown in Figure 1 (red curve) is quite similar to that observed in CH_2Cl_2.

It is known that for some amphiphilic C_{60} derivatives[39] the sharp peak around 430 nm is sensitive to the solution parameters, e.g., concentration. Above a critical concentration aggregation may occur, leading to increased $\pi-\pi$ interactions between C_{60} moieties. Once this happens, the sharp peak becomes broader and the Lambert−Beer rule no longer applies.[40] As already noted, due to the intrinsic polarity difference between C_{60} and aliphatic chains, the alkylated fullerenes can be regarded as unique amphiphiles in organic solvents.[17] To determine whether **1** and **2** form aggregates, the absorption band around 430 nm was monitored as a function of concentration in CH_2Cl_2. No peak shift or peak broadening is observed, and the absorption obeys the Lambert−Beer rule within the concentration range studied (Figure S1). Similarly, in a MeOH/CH_2Cl_2 mixed solvent with a MeOH volume content of 10%, no aggregation was detected up to 500 μM (Figure 2A). However, aggregation of **1** was noted in samples with higher MeOH content, i.e., increased solvent polarity. A significant absorption decrease at constant concentration of **1** was observed when the MeOH content exceeded 50 vol % (Figure 2B). The aggregation behavior of **1** in the mixed MeOH/CH_2Cl_2 solvent conditions has been studied (*vide infra*).

Electrochemical Properties. The introduction of an ionic part induced changes in the redox properties of the molecule, as revealed by electrochemical measurements. In homogeneous solution state with CH_2Cl_2 as a solvent, four reduction peaks were observed for **1** located at −0.97, −1.36, −1.85, and −2.20 V (*E* vs Fc/Fc^+), respectively (Figure 3A, curves a and b). Under the same experimental conditions, only three reduction peaks were detected for **2** located at −1.12, −1.52, and −2.04 V, respectively (Figure 3A, curve c). The positive shifts of the reduction peaks indicate that it is easier for **1** to get electrons compared to **2** and that its HOMO−LUMO level is lower. This is consistent with the results reported for other fulleropyrrolidinium species, which showed similar trends in THF[41] or aqueous[42] solutions.

Interestingly, these positive potential shifts of the reduction peaks can also happen in the film state, the analysis of which has been carried out in an aqueous electrolyte solution. As shown in Figure 3B, two reduction peaks at −0.42 and −0.81 V (*E* vs Ag/AgCl) are observed for a cast film of **1** at 70 °C, while they locate at −0.71 and −0.88 V for the film of **2** measured at the same temperature, as reported previously.[21] The temperature condition applied here is above the crystal to liquid crystal phase transition temperatures for both **1** and **2** (see DSC results discussed later and shown in Figure S4). Under such condition the fluidity of the films is much higher than in the crystal state, which is known to help the diffusion of substances including water, supporting electrolytes, and C_{60} molecules themselves. Unlike the electrochemical behavior in homogeneous solution where the signal can be stable for multiple scans, a continuous decrease of peak intensity was observed, presumably due to the formation of an electrochemically inert film upon continuous scan.[43]

Self-Assembly Behavior. One of the fascinating aspects of alkylated fullerenes is their self-assembly[44] both from solution and on substrates. They have been shown to self-organize into a variety of supramolecular architectures such as three-dimensional hierarchically organized meso/microscopic objects[16,19] or one-dimensional epitaxially grown fullerene nanowires.[20] This unusual self-assembly behavior is dictated by the fine balance of intermolecular forces, e.g., $\pi-\pi$ (C_{60} molecules) and van der Waals (alkyl chains) interactions in changing assembly environments, e.g., solvent conditions or structured substrates. To explore the influence of the introduction of an ionic part on

dx.doi.org/10.1021/la2015176 |*Langmuir* 2011, 27, 7493–7501

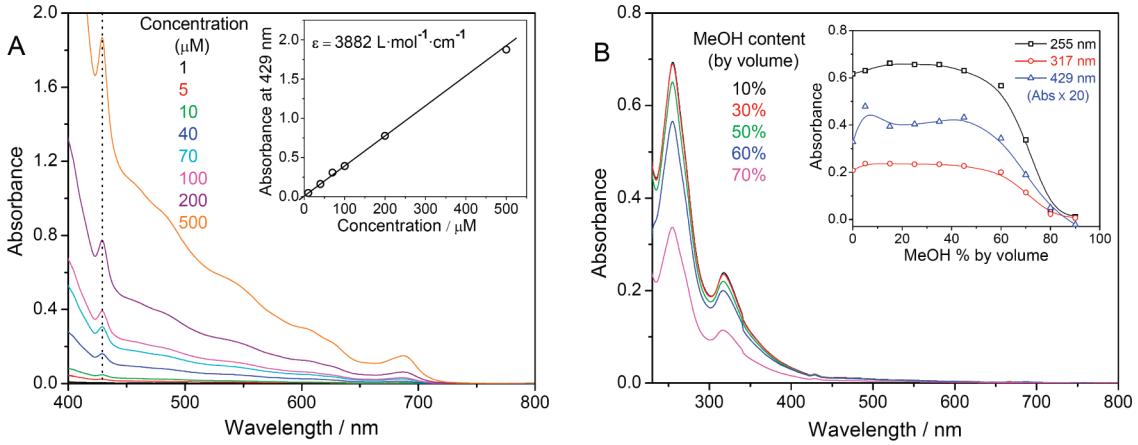

Figure 2. (A) Absorption of **1** in the visible region in a MeOH/CH_2Cl_2 mixed solvent with a MeOH volume content of 10% at different concentrations. Inset shows the absorption−concentration relationship for the peak at 429 nm (the correlation coefficient to linear plot is 0.9994). (B) Selected spectra of 5 μM **1** in MeOH/CH_2Cl_2 mixed solvent at different MeOH contents. Inset shows the absorption changes for the three main peaks as a function of MeOH content.

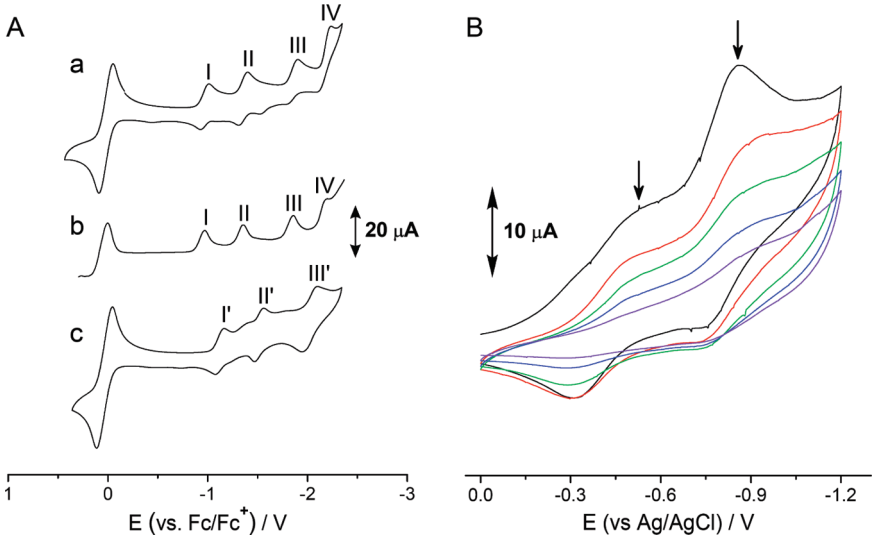

Figure 3. (A) Cyclic voltammogram (CV) (a) and differential pulse voltammogram (b) of **1** evaluated in CH_2Cl_2 at room temperature. For comparison, CV of **2** (c) is given. Solution contains 0.5 mM ferrocene as internal reference and 0.1 M $TBABF_4$ as supporting electrolyte. The concentration of **1** and **2** is fixed at 0.5 mM. Scan rate is 0.1 V/s. (B) CV of **1** in film state at 70 °C in 0.1 M aqueous TBACl solution. Five scan circles are given. The film was prepared from drying a 1 mM CH_2Cl_2 solution (10 μL) of **1** on a glassy carbon electrode. Scan rate is 0.1 V/s.

the molecular organization, the self-assembly behavior of **1** has been investigated. A simple heating−cooling cycle from 1,4-dioxane was previously applied for the production of flakelike microparticles from **2**. Unfortunately, this method failed to produce well-structured architectures from **1**, probably due to the lower solubility of **1** in 1,4-dioxane (<0.25 mM) compared to that of **2** (>3 mM) at 70 °C.

As an alternative assembly strategy, liquid−liquid interfacial precipitation (LLIP) has been widely exploited to produce pristine C_{60} crystals with a variety of shapes.[45] Typically a poor solvent is added above a solution of the molecule of interest in a good solvent, and self-assembly happens preferentially at the interface. By slowly adding excess MeOH to on top of a concentrated CH_2Cl_2 solution of **1**, self-organized microparticles possessing flakes with roughness on the nanometer length scale could be produced (Figure 4a−c). It has been accepted that hierarchically organized rough surfaces tend to show enhanced hydrophobic properties.[46−48] The absolute wettability depends on the roughness and molecular component of the surfaces. Possessing both a hierarchically organized rough surface and intrinsic hydrophobic properties, assemblies of **2** have been found to exhibit superhydrophobicity, with a static water contact angle around 150°.[16,19] To investigate the influence of the additional ionic part in **1** on the wettability, an investigation on the film made from microparticles of **1** (Figure 4a−c) was carried out. A static water contact angle of 140 ± 3° was found (Figure 4d). Despite this value being ∼10° lower than that for **2**, it is clear that microparticles of **1** still retain a relatively high water repellency despite the presence of the ionic unit. The reduction in contact angle could be due to different surface roughness in particles formed by **1** and **2**, but we speculate that it is more likely to be due to the presence of the ionic unit. Indeed, in a previous study we proposed a hypothesis that under polar solvent conditions the C_{60} moiety remains outside of the

dx.doi.org/10.1021/la2015176 |*Langmuir* 2011, 27, 7493–7501

assemblies and in contact with the solvent while the alkyl chains stay inside.[16,19,49] It therefore follows that since the ionic part of **1** is close to the C_{60} moiety, the outer surface of the self-assembled microparticles of **1**, prepared using the polar mixed MeOH/CH_2Cl_2 solvent, is likely to be more hydrophilic compared to those of **2**. This accounts for the slightly lower water contact angle and adds further evidence to our hypothesis. The hydrophilicity of the iodide counterion is clearly insufficient to reduce the high hydrophobicity of the assemblies.

Figure 5A shows SAXS data from a powder sample of the obtained microparticles. Clear peaks are observed in the scattering, which suggest that **1** adopts a multilamellar arrangement with a typical spacing of order 4.8 nm. This is similar to the structure of related systems elucidated by XRD,[16,19,21] and the peak labeling in Figure 5A is in line with those results. A simple molecular Corey–Pauling–Koltun (CPK) space-filling modeling of **1** suggests a length of 3.7 nm in a fully extended conformation. As the interlayer distance revealed by SAXS is far less than twice this value, the alkyl chains of two neighboring layers probably interpenetrate each other and/or are tilted within the lamellae. In addition, judging from FT-IR analysis (Figure 5B), the alkyl chain moieties of **1** are slightly disordered. The asymmetric and symmetric methylene stretching modes appeared at 2921 and 2851 cm^{-1} for **1**, whereas they are seen at 2918 and 2849 cm^{-1}, respectively, for **2**.[19] The values for **2** were assigned to an *all-trans* conformation of the oligomethylene units. However, the peaks for **1** are shifted to lower wavenumbers, suggesting that the alkyl chains contain some gauche conformation and therefore have a lower degree of crystallinity. It is likely that the crystallinity has been partially disturbed by the addition of the ionic component of **1**. An additional information noted from the IR comparison is that the peak at 2780 cm^{-1} observed in **2** is absent in **1**. This is presumably due to the limited methylene stretching motion in the pyrrolidine ring after quaternization.

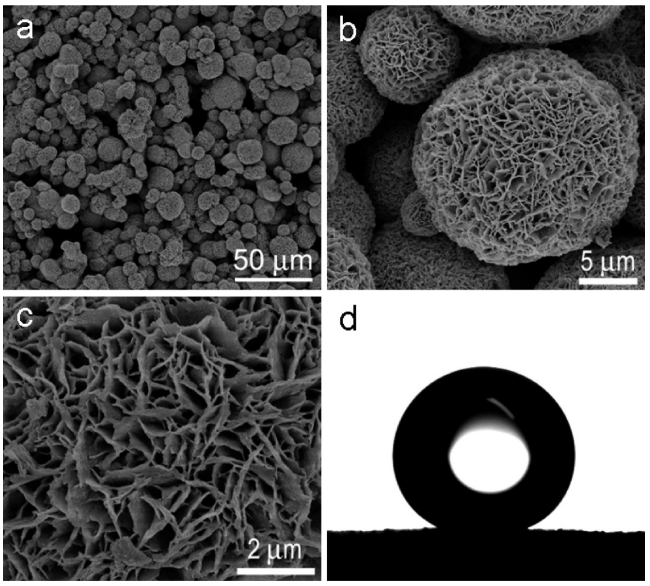

Figure 4. Typical SEM images (a–c) at different magnifications of flakelike microparticles of **1** precipitated by slowly adding excess MeOH to a concentrated CH_2Cl_2 solution of **1**. A photograph (d) of a water droplet on the surface in which shows static water contact angle is 140 ± 3°.

Besides the precipitation method, different self-assembly behavior was also observed by simply casting a stock solution of **1** onto a silicon substrate. When a solution of **1** in CH_2Cl_2 with concentrations between 0.5 and 1.0 mM is drop-cast onto a silicon wafer and the solvent is allowed to evaporate, a film with some cracks was observed (Figure 6a). In contrast, when a 1 mM solution of **2** in CH_2Cl_2 or a MeOH/CH_2Cl_2 mixture is drop-cast on a silicon substrate, microparticles composed of flakes were obtained (Figure S2). This indicates that the introduction of an ionic part strongly affects the self-assembly phenomena under similar solvent conditions. This may result from the fact that the alkyl chains in **1** are not able to crystallize as well as those in **2**, as suggested by FT-IR. However, when mixed solvents of MeOH/CH_2Cl_2 are applied, the self-assembly behavior of **1** depends on the MeOH content. Here the concentration of **1** was fixed as 0.5 mM, and the solutions were drop-cast onto a silicon substrate. In 10 vol % MeOH in CH_2Cl_2, the resulting assemblies were closely packed flowerlike objects of micrometer dimensions (Figure 6b). Further increase in MeOH content yielded doughnut-shaped micro-objects with rough surfaces (Figure 6c,d). These structures persisted until the MeOH content reached 50 vol %, beyond which low solubility of **1** in the solvent mixture

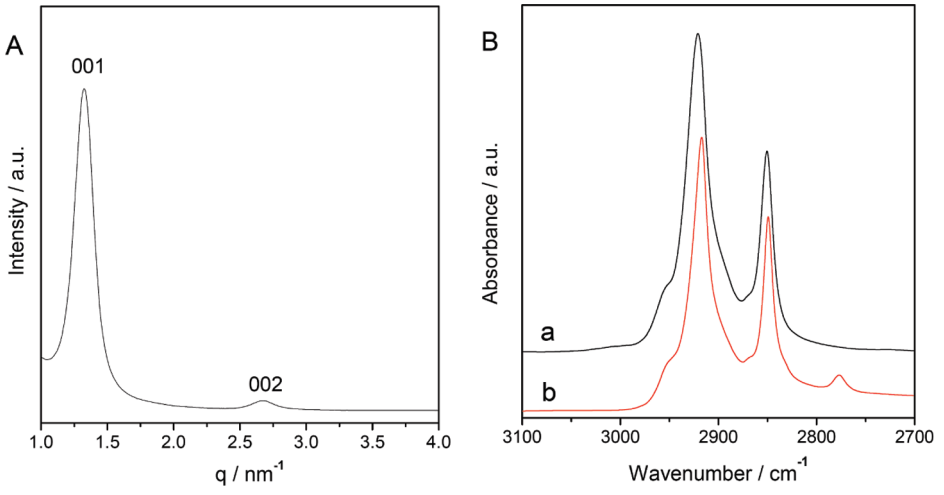

Figure 5. (A) Small-angle X-ray scattering (SAXS) of flakelike microparticles of **1**. (B) FT-IR spectra of **1** (a) and **2** (b). Both SAXS and FT-IR were recorded at room temperature.

dx.doi.org/10.1021/la2015176 |*Langmuir* 2011, 27, 7493–7501

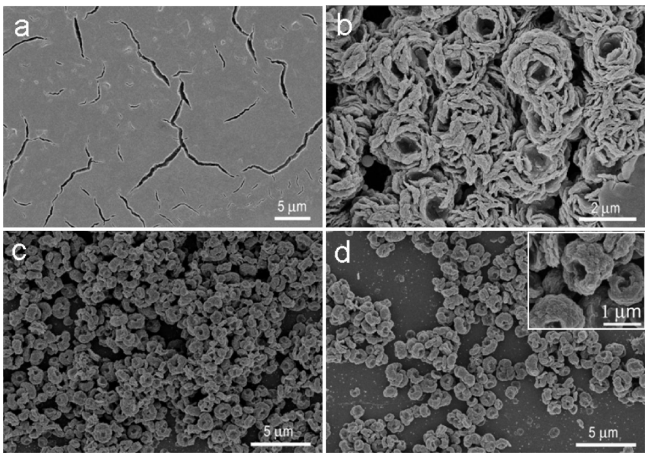

Figure 6. Typical SEM images of the self-organized structures of **1** formed on silicon substrates by evaporating a 0.5 mM solution in MeOH/CH_2Cl_2 mixed solvent with a MeOH volume content of 0 (a), 10% (b), 20% (c), and 30% (d). Inset of (d) is the magnification of the doughnut-shaped objects.

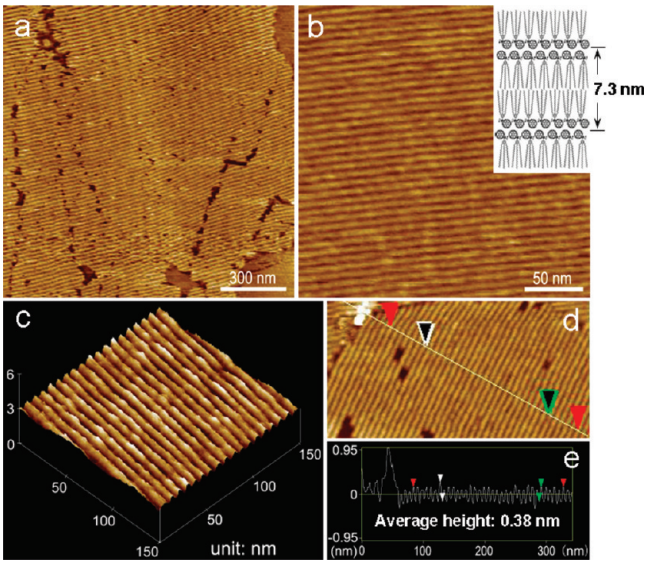

Figure 7. Typical AFM images by spin-coating a 10 μM CH_2Cl_2 solution of **1** on HOPG. (a, b) Images taken at different magnifications. Inset of (b) is a schematic illustration of the molecular arrangement within the nanowires. A typical height image (c) and cross-sectional analysis (d, e) of the nanowires are also shown.

prevented sample preparation. It is worth noting from these self-assembly studies that **1** displayed supramolecular polymorphism under different assembly conditions. While similar phenomenon were observed in the self-assembly of **2**, the presence of an ionic component has allowed the expansion of the polymorphic features. Additionally, it has improved our understanding of the outer surface component of self-organized microparticles prepared in polar solvents.

Nanowire Formation. One promising self-assembly of molecules that bear long alkyl chains is an epitaxially grown submonolayer film with the support of surface lattice structures of highly periodic substrates.[50] When a 10 μM CH_2Cl_2 solution of **1** is spin-coated on highly oriented pyrolytic graphite (HOPG), perfectly straight fullerene nanowires were observed under AFM at ambient conditions (Figure 7). The periodic separation of the nanowires is 7.3 nm, which is almost exactly twice the molecular length of **1** in a fully extended conformation (3.7 nm, see above). This value is similar to that shown by **2**, which is 7.2 nm.[20] In addition, a cross-sectional line analysis reveals that the average height difference within the lamellae is 0.38 nm, which is close to the difference between the diameter of C_{60} and the height of a flat-lying alkyl chain layer on the HOPG surface. These results indicate that the organization of **1** within nanowires is similar to that of **2**,[20] with the C_{60} moieties organized in a zigzag conformation and the aliphatic chains localized in between.

Extremely large areas of two-dimensional lamellar domains composed of the C_{60} nanowires with lengths of over 1.0 μm were noted by AFM (Figure 7a and Figure S3). While nanowire formation for both **1** and **2** is likely to be driven by the alignment of the epitaxially crystallized alkyl chains on the HOPG lattice[50] and $\pi-\pi$ interaction between C_{60} moieties, in the case of **1**, an additional electrostatic interaction is present. This may greatly contribute to the stability of the nanowires and account for the existence of extremely long nanowires, possibly by the formation of salt bridges between neighboring ionic moieties. To the best of our knowledge, the nanowires formed by **1** as shown here are the longest class of one-dimensional self-assemblies not only for fullerenes[51] but also for other functional molecules[52] analyzed by AFM.

Thermotropic Properties. Although various fulleropyrrolidinium compounds have been synthesized to date, there have been no detailed investigations into their thermotropic properties. One possible explanation for this is that due to their enhanced water solubility, the majority of interest in such molecules has been focused on their biological activities, which are normally evaluated at room temperature. To account for this neglect, the thermotropic behavior of **1** has been investigated in detail. First, thermogravimetric analysis (TGA) on **1** was carried out and the result is given in Figure 8a. Significant weight loss was observed above 350 °C (region II). Below 350 °C, a small weight loss of 4.5% was also noticed (region I). Differential scanning calorimetry (DSC) was performed with an upper temperature limit of 200 °C and a scan rate of 10 °C/min. Under this condition, a crystal to liquid crystal phase transition at 60 °C and a liquid crystal to isotropic phase transition at 188 °C were observed (Figure S4). No obvious peak shifts were found upon multiple scans of up to three cycles, indicating that **1** is fairly stable under such conditions. When the maximum temperature reaches a higher limit (e.g., 250 °C), peak shifts were noticed upon multiple scans, suggesting the thermal decomposition of **1**. The transition temperatures of crystal/liquid crystal and liquid crystal/isotropic liquid for **1** are 1.5 and 5 °C lower, respectively, in comparison to those for **2**.[21] This could be due to the fact that the crystallinity of the aliphatic chains are slightly disturbed upon ionization (see the FT-IR discussion and Figure 5B).

Ionic liquid crystals containing π-conjugated units are interesting examples for optoelectronic applications due to their efficient carrier injection from the electrode and carrier transporting ability.[31] Upon cooling from the isotropic phase of **1** below its melting point, textures typical of a smectic phase were observed under a polarized optical microscope (POM) (Figure 8b). XRD data obtained at 170 °C revealed a typical lamellar organization of the mesophase with a periodic distance of 5.6 nm (Figure 8c). Here diffraction peaks up to the (004) plane were observed, together with halos corresponding to molten states of C_{60} (2θ = ~10°) and alkyl chains (2θ = ~18°). The *d*-spacing value is lower than twice of the full extended conformation of **1** but bigger than

dx.doi.org/10.1021/la2015176 |*Langmuir* 2011, 27, 7493–7501

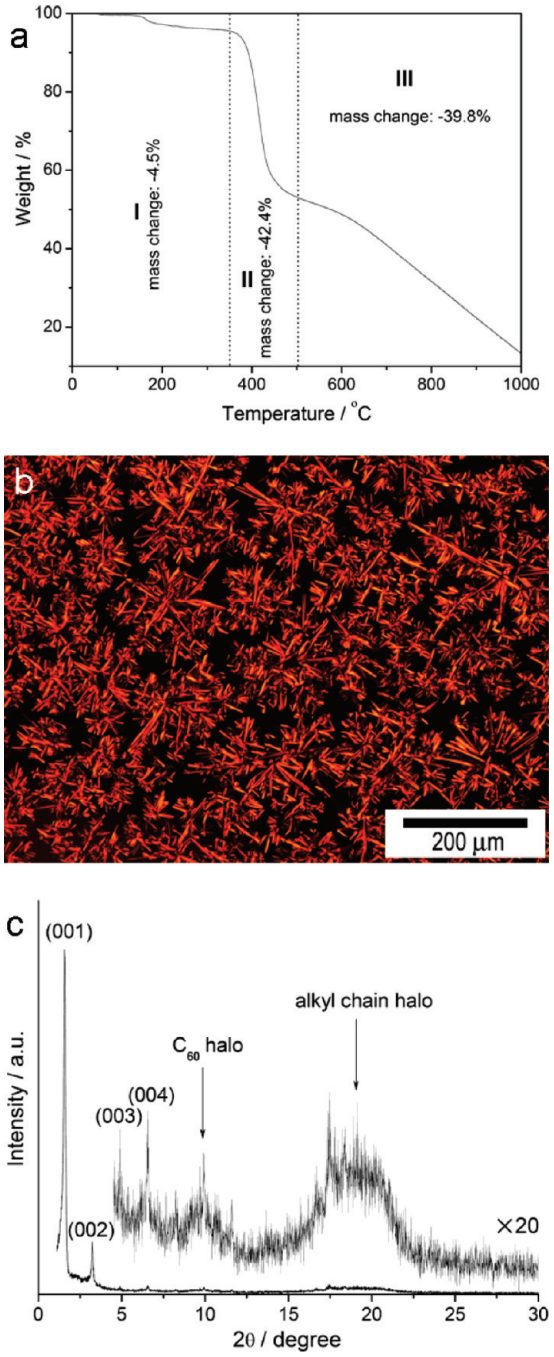

Figure 8. TGA (a) of **1** with a heating rate of 10 °C/min. A typical polarized optical microscopy (POM) image (b) of **1** at 170 °C upon cooling from isotropic melt at 1 °C/min. XRD pattern (c) of **1** at 170 °C.

the lamellar distance in the microparticles revealed by SAXS at room temperature (4.8 nm). We speculate that in the mesophase the alkyl chains are rather disordered and may be still in an interdigitated state. This would be the first fulleropyrrolidinium liquid crystalline material.

A concern in the thermotropic behavior of **1** is the multiple step weight loss observed in the TGA (Figure 8a). Indeed, the thermotropic behavior of **1** is rather complicated compared to that of **2**, which only shows significant weight loss above 350 °C. In order to better understand this, **1** was subjected to treatment at elevated temperatures until obvious decomposition was observed via TLC monitoring. During this experiment another component is generated with a higher R_f value. This component was isolated and evaluated by ^{1}H NMR, which showed it to be the neutral fulleropyrrolidine **2** (Figure S5). A back-reaction from **1** to **2** has therefore occurred, leading to the deionization of **1**. To test whether this is a universal feature of alkylated fulleropyrrolidinium compounds, C_{60} derivatives with different number and type of aliphatic chains as well as with different counterions (see chemical structures in Scheme S1) were prepared. It was found that similar thermal decomposition phenomena took place in all cases. It is known that quaternary ammonium salts of lower molecular weights can undergo a back-reaction and regenerate neutral amines via S_N2 substitution or Hoffmann elimination upon heating.[53−55] Since a β-hydrogen is absent in **1**, it is likely that **1** was deionized to its neutral species **2** via a S_N2 substitution (Scheme S2).

It should be pointed out that the deionization is driven kinetically. It is known that deionization temperatures of common quaternary ammonium salts are typically over 200 °C. In case of **1**, however, the temperature needed for the deionization is found to be much lower. Even at room temperature, the back-reaction from **1** to **2** has been observed after several months storage in the dark. It can be ascribed to the low basicity of the nitrogen on the fulleropyrrolidine ring induced by the presence of the electron deficient C_{60} moiety.[35,36] This leads to a weak nucleophilicity of the fulleropyrrolidines and makes the quaternization reaction to fulleropyrrolidiniums more difficult than common quaternary ammonium salts. Once fulleropyrrolidines are quaternized to fulleropyrrolidinium salts, the strength of the newly formed C−N bond on the pyrrolidinium ring will be weaker, accounting for this result.

However, the deionization process is not simple. We found the kinetics of the back-reaction to depend on a variety of factors including the decomposition temperature and time as well as the presence or absence of light illumination. In many cases when the mixture after thermal decomposition was evaluated by TLC, other components could also be observed besides the bands of **1** and **2**. This means the back-reaction is potentially accompanied by other side reactions. Considering that the thermal deionization of polydialkyldimethylammonium chloride is already complicated,[56] this complexity for the deionization of **1** is understandable given the presence of the additional π-conjugate system (C_{60}). Among the possible side reactions of thermal decomposition, formation of C_{60} zwitterions via charge transfer from I^- to the C_{60} moiety may occur. Under certain circumstances we have observed a band on silica column chromatography besides **1** and **2** with a red color, which is presumably I_2. To fully reveal this complexity is out of the scope of current work, and further efforts are needed to fulfill this task in the future.

CONCLUSIONS

In summary, we have synthesized a novel fulleropyrrolidinium **1** that carries an ionic moiety and long aliphatic chains from its neutral precursor **2**. The spectroscopic and redox features, self-assembly, and thermotropic properties of **1** have been investigated in detail in comparison to those of **2**. The introduction of the ionic part induces obvious changes in the electronic structures of the C_{60} moiety. **1** shows versatile self-organization including the formation of hierarchically organized microparticles with water-repellent properties and ultralong perfectly straight fullerene nanowires on graphite. The presence of the

ionic part introduces advantageous properties to **1**, which may be explained by the salt bridge effect among the ionic moieties with a combination of other intermolecular interactions including $\pi-\pi$ between C_{60} moieties and van der Waals forces among alkyl chains. One possibility is the alignment of negatively charged molecules such as DNA and polymers along the perfectly straight C_{60} nanowires. It would be interesting to study the photoinduced DNA cleavage by C_{60} in such a system.

The advantage of the "ionic" alkylated fullerene derivatives is their versatile ability to form variously structured and morphological self-assembled materials, which are carried from the similar intrinsic nature of their neutral derivative and significantly have never before been obtained from ionic fullerenes. In addition, the salt-bridge effect in the nanowire assembly originates from the additional ionicity. This is a good demonstration that "ionic" alkylated fullerene derivatives can be categorized as novel ionic supramolecular substances for developing multifunctional self-assembly soft materials.

Although the thermal stability needs to be improved before any further real application can be found, the first fulleropyrrolidinium liquid crystalline material has been developed. In addition, new insights toward the deionization reactions from fulleropyrrolidiniums to the corresponding fulleropyrrolidines have been noticed. Besides further encouraging fullerene science, this result can also serve as a useful reference for those who want to invest more on fulleropyrrolidinium compounds. Moreover, our result also serves as a kind reminder to those studying the use of water-soluble fulleropyrrolidiniums for biological tests, where careful examination on long-term stability is usually lacking.

■ ASSOCIATED CONTENT

Supporting Information. UV−vis absorptions, SEM and AFM images, ^{1}H NMR and DSC results, and molecular structures of alkylated ionic fullerenes. This material is available free of charge via the Internet at http://pubs.acs.org.

■ AUTHOR INFORMATION

Corresponding Author

*E-mail: NAKANISHI.Takashi@nims.go.jp. Fax: +81 29 859 2101. Tel: +81 29 860 4740.

■ ACKNOWLEDGMENT

This work was supported, in part, by KAKENHI, MEXT, Japan, and "PRESTO", JST, Japan as well as the Shorai Foundation. We thank Dr. Takeuchi (NIMS) as well as Dr. Asanuma (MPI) for the meaningful discussions.

■ REFERENCES

(1) Babu, S. S.; Möhwald, H.; Nakanishi, T. *Chem. Soc. Rev.* **2010**, *39*, 4021.
(2) Deibel, C.; Dyakonov, V. *Rep. Prog. Phys.* **2010**, *73*, 096401.
(3) Bonifazi, D.; Enger, O.; Diederich, F. *Chem. Soc. Rev.* **2007**, *36*, 390.
(4) Martn, N. *Chem. Commun.* **2006**, 2093.
(5) Nakamura, E.; Isobe, H. Y. *Acc. Chem. Res.* **2003**, *36*, 807.
(6) Li, W.-S.; Yamamoto, Y.; Fukushima, T.; Saeki, A.; Seki, S.; Tagawa, S.; Masunaga, H.; Sasaki, S.; Takata, M.; Aida, T. *J. Am. Chem. Soc.* **2008**, *130*, 8886.
(7) Ariga, K.; Hill, J. P.; Lee, M. V.; Vinu, A.; Charvet, R.; Acharya, S. *Sci. Technol. Adv. Mater.* **2008**, *9*, 014109.
(8) Maggini, M.; Scorrano, G.; Prato, M. *J. Am. Chem. Soc.* **1993**, *115*, 9798.
(9) Campidelli, S.; Lenoble, J.; Barberá, J.; Paolucci, F.; Marcaccio, M.; Paolucci, D.; Deschenaux, R. *Macromolecules* **2005**, *38*, 7915.
(10) Mashino, T.; Okuda, K.; Hirota, T.; Hirobe, M.; Nagano, T.; Mochizuki, M. *Bioorg. Med. Chem. Lett.* **1999**, *9*, 2959.
(11) Bosi, S.; Ros, T. D.; Castellano, S.; Banfi, E.; Prato, M. *Bioorg. Med. Chem. Lett.* **2000**, *10*, 1043.
(12) Guldi, D. M.; Luo, C.; Kotov, N. A.; Ros, T. D.; Bosi, S.; Prato, M. *J. Phys. Chem. B* **2003**, *107*, 7293.
(13) Luo, C.; Guldi, D. M.; Maggini, M.; Menna, E.; Mondini, S.; Kotov, N. A.; Prato, M. *Angew. Chem., Int. Ed.* **2000**, *39*, 3905.
(14) Masuda, K.; Abe, T.; Benten, H.; Ohkita, H.; Ito, S. *Langmuir* **2010**, *26*, 13472.
(15) Nakanishi, T. *Chem. Commun.* **2010**, *46*, 3425.
(16) Nakanishi, T.; Shen, Y.; Wang, J.; Li, H.; Fernandes, P.; Yoshida, K.; Yagai, S.; Takeuchi, M.; Ariga, K.; Kurth, D. G.; Möhwald, H. *J. Mater. Chem.* **2010**, *20*, 1253.
(17) Asanuma, H.; Li, H.; Nakanishi, T.; Möhwald, H. *Chem.—Eur. J.* **2010**, *16*, 9330.
(18) Nakanishi, T.; Schmitt, W.; Michinobu, T.; Kurth, D. G.; Ariga, K. *Chem. Commun.* **2005**, 5982.
(19) Nakanishi, T.; Michinobu, T.; Yoshida, K.; Shirahata, N.; Ariga, K.; Möhwald, H.; Kurth, D. G. *Adv. Mater.* **2008**, *20*, 443.
(20) Nakanishi, T.; Miyashita, N.; Michinobu, T.; Wakayama, Y.; Tsuruoka, T.; Ariga, K.; Kurth, D. G. *J. Am. Chem. Soc.* **2006**, *128*, 6328.
(21) Nakanishi, T.; Shen, Y.; Wang, J.; Yagai, S.; Funahashi, M.; Kato, T.; Fernandes, P.; Möhwald, H.; Kurth, D. G. *J. Am. Chem. Soc.* **2008**, *130*, 9236.
(22) Nakanishi, T.; Morita, M.; Murakami, H.; Sagara, T.; Nakashima, N. *Chem.—Eur. J.* **2002**, *8*, 1641.
(23) Murakami, H.; Nakanishi, T.; Morita, M.; Taniguchi, N.; Nakashima, N. *Chem.—Asian J.* **2006**, *1*, 860.
(24) Patnaik, A. *J. Nanosci. Nanotechnol.* **2007**, *7*, 1111.
(25) Yang, X.; Zhang, G.; Zhang, D.; Xiang, J.; Yang, G.; Zhu, D. *Soft Matter* **2011**, *7*, 3592.
(26) Sawamura, M.; Kawai, K.; Matsuo, Y.; Kanie, K.; Kato, T.; Nakamura, E. *Nature* **2002**, *419*, 702.
(27) Horii, Y.; Sakaguchi, K.; Chikamatsu, M.; Azumi, R.; Yase, K.; Kitagawa, M.; Konishi, H. *Appl. Phys. Express* **2010**, *3*, 101601.
(28) Binnemans, K. *Chem. Rev.* **2005**, *105*, 4148.
(29) Kouwer, P. H. J.; Swager, T. M. *J. Am. Chem. Soc.* **2007**, *129*, 14042.
(30) Zakrevskyy, Y.; Stumpe, J.; Faul, C. F. J. *Adv. Mater.* **2006**, *18*, 2133.
(31) Yazaki, S.; Funahashi, M.; Kato, T. *J. Am. Chem. Soc.* **2008**, *130*, 13206.
(32) Mukai, K.; Asaka, K.; Sugino, T.; Kiyohara, K.; Takeuchi, I.; Terasawa, N.; Futaba, D. N.; Hata, K.; Fukushima, T.; Aida, T. *Adv. Mater.* **2009**, *21*, 1582.
(33) Maeda, H.; Haketa, Y.; Nakanishi, T. *J. Am. Chem. Soc.* **2007**, *129*, 13661.
(34) Taubert, A. *Angew. Chem., Int. Ed.* **2004**, *43*, 5380.
(35) D'Souza, F.; Zandler, M. E.; Deviprasad, G. R.; Kutner, W. *J. Phys. Chem. A* **2000**, *104*, 6887.
(36) Bagno, A.; Claeson, S.; Maggini, M.; Martini, M. L.; Prato, M.; Scorrano, G. *Chem.—Eur. J.* **2002**, *8*, 1015.
(37) Bensasson, R. V.; Bienvenüe, E.; Fabre, C.; Janot, J. M.; Land, E. J.; Leach, S.; Leboulaire, V.; Rassat, A.; Roux, S.; Seta, P. *Chem.—Eur. J.* **1998**, *4*, 270.
(38) Leach, S.; Vervloet, M.; Desprès, A.; Bréheret, E.; Hare, J. P.; Dennis, T. J.; Kroto, H. W.; Taylor, R.; Walton, D. R. M. *Chem. Phys.* **1992**, *160*, 451.
(39) Guldi, D. M.; Hungerbiihler, H.; Asmus, K.-D. *J. Phys. Chem. B* **1999**, *103*, 1444.
(40) Texier, I.; Berberan-Santos, M. N.; Fedorov, A.; Brettreich, M.; Schönberger, H.; Hirsch, A.; Leach, S.; Bensasson, R. V. *J. Phys. Chem. A* **2001**, *105*, 10278.

(41) Ros, T. D.; Prato, M.; Carano, M.; Ceroni, P.; Paolucci, F.; Roffia, S. *J. Am. Chem. Soc.* **1998**, *120*, 11645.
(42) Guldi, D. M. *J. Phys. Chem. B* **2000**, *104*, 1483.
(43) Nakashima, N.; Ishii, T.; Shirakusa, M.; Nakanishi, T.; Murakami, H.; Sagara, T. *Chem.—Eur. J.* **2001**, *7*, 1766.
(44) Charvet, R.; Acharya, S.; Hill, J. P.; Akada, M.; Liao, M.; Seki, S.; Honsho, Y.; Saeki, A.; Ariga, K. *J. Am. Chem. Soc.* **2009**, *131*, 18030.
(45) Miyazawa, K.; Kuwasaki, Y.; Obayashi, A.; Kuwabara, M. *J. Mater. Res.* **2002**, *17*, 83.
(46) Sun, T.; Feng, L.; Gao, X.; Jiang, L. *Acc. Chem. Res.* **2005**, *38*, 644.
(47) Onda, T.; Shibuichi, S.; Satoh, N.; Tsujii, K. *Langmuir* **1996**, *12*, 2125.
(48) Wang, J.; Shen, Y.; Kessel, S.; Fernandes, P.; Yoshida, K.; Yagai, S.; Kurth, D. G.; Möhwald, H.; Nakanishi, T. *Angew. Chem., Int. Ed.* **2009**, *48*, 2166.
(49) Yang, L.; Shirahata, N.; Saini, G.; Zhang, F.; Pei, L.; Asplund, M. C.; Kurth, D. G.; Ariga, K.; Sautter, K.; Nakanishi, T.; Smentkowshi, V.; Linford, M. R. *Langmuir* **2009**, *25*, 5674.
(50) Rabe, J.; Buchholz, S. *Science* **1991**, *12*, 424.
(51) Feng, M.; Lee, J.; Zhao, J.; Yates, J. T.; Petek, H., Jr. *J. Am. Chem. Soc.* **2007**, *129*, 12394.
(52) Crivillers, N.; Furukawa, S.; Minoia, A.; Heyen, A. V.; Mas-Torrent, M.; Sporer, C.; Linares, M.; Volodin, A.; Haesendonck, C. V.; Auweraer, M. V.; Lazzaroni, R.; Feyter, S. D.; Veciana, J.; Rovira, C. *J. Am. Chem. Soc.* **2009**, *131*, 6246.
(53) Sharma, R. K.; Fry, J. L. *J. Org. Chem.* **1983**, *48*, 2112.
(54) Galimberti, M.; Martino, M.; Guenzi, M.; Leonardi, G.; Citterio, A. *e-Polym.* **2009**, *no. 056*.
(55) Sawicka, M.; Storoniak, P.; Skurski, P.; Błażejowski, J.; Rak, J. *Chem. Phys.* **2006**, *324*, 425.
(56) Francis, S.; Varshney, L.; Sabharwal, S. *Eur. Polym. J.* **2007**, *43*, 2525.